UNIVERSITY OF BIRMINGHAM

University of Birmingham

School Of Physics and Astronomy

Fourth Year Project

Modelling Stochastic Noise in AGN: A Critical Analysis of Super Massive Black Hole Binary Claims

Author:
Nicholas Kinsey

Supervisor:
Dr. W Farr

Student Number: 1323800

Word Count: 8768

June 22, 2017

Abstract

Hierarchical models of galaxy formation predict the existence of Super-Massive Black Hole (SMBH) binaries. Claims regarding the discovery of such phenomenon at close (sub-parsec) separations have been made by observing an underlying periodicity in the intensity variations of 'Active Galactic Nuclei' (AGN) objects over time. For the critical analysis performed here, focus is placed on the 111 identified periodic candidates by Graham et al. (2015) and the given 'best performing candidate' in their analysis: "PG 1302-102". [1] [2] This investigation assesses SMBH binary claims through the application of a Continuous-time Auto-Regressive Moving Average (CARMA) modelling technique, on both the 111 Graham et al. periodic candidates and 312 randomly selected (presumed non-binary) AGN objects. Through direct comparisons of the model outputs, this investigation contradicts the results of Graham et al. (2015), in that strong periodic behaviour is not observed in the identified periodic candidates, with object 'PG 1302-102' performing relatively poorly. Implementation of this CARMA modelling technique on a large dataset in order to identify other SMBH binary candidates is not performed here, but is highly encouraged for future studies.

Contents

1 Introduction

This report outlines a methodology implemented in order to critically analyze the recent claims being put forward in the astrophysics community regarding the identification of sub-parsec Super-Massive Black Hole (herein SMBH) binary candidates. The identification of such an object is pivotal in advancing our understanding regarding galactic evolution and mergers, as, it would allow for observations of the final moments of a successful galactic merger to take place. Currently, this area of astrophysics is not well understood, it is hoped that the recent discovery of Gravitational Waves (GWs) by the LIGO project will eventually enable us to detect SMBHs directly, of which a SMBH binary is an intense, high frequency source. [3] The identification of SMBH binaries will further enhance our understanding of the processes involved in galactic mergers, furthermore, fundamental differences in the physical properties of binary and non-binary SMBHs may be investigated thoroughly as a result.[4]

In recent years, there has been a rapid increase in Large Time-Domain Surveys (LTDS), such as the Catalina Real-time Transient Survey (CRTS), which was utilized in the completion of this project. [5] Such surveys collect huge amounts of astronomical flux measurements for a large number of objects at different time intervals, hence allowing them to display this data in the form of light-curves (relative flux magnitude against time). Due to the recent availability of such data, many claims have been made regarding the identification of quasar candidates who appear to have an underlying periodicity in their associated light-curves, such a phenomenon is indicative of a sub-parsec SMBH binary system, as outlined in section 1.1. In particular, this report focuses on the claims put forward by Graham et al. (2015) [1] [2] and the subsequent analysis performed by Vaughan et al. (2016). [6] Although, many others have also used various different analytical methods to identify such objects, [7] the focus of this project has revolved around evaluating the results attained by Graham et al. (2015) as these results are recent and widely accepted.

1.1 Physical Processes Governing AGN Evolution

From current hierarchical models of galaxy formation, SMBH binaries are predicted to exist and form a significant proportion of the total AGN population. [8] It is thought that such an object may arise from the merger of two galaxies, whereby the two SMBHs orbit each other at a large separation, which slowly reduces as the binary pair emit radiation through a variety of physical processes. [9] Notably, SMBH binary systems have been detected at *kpc* separations, however, the resolution limit of telescopes prevents observations of sub-parsec SMBH binary systems. [10] At a separation of approximately 1 *pc*, the rate of coalescence of the binary pair slows, this phenomenon is know as the 'final parsec problem'. [11] As a result, a significant proportion of the binary AGN population is expected to exist within a sub-parsec separation. A conclusive identification of a sub-parsec SMBH binary object is required to enhance investigations which explore the underlying physical mechanisms of galactic mergers. Furthermore, a SMBH binary is thought to be an intense source of nano-hertz frequency Gravitational Waves, hence, such objects may be probed by a space-based gravitational wave detector. [12]

Currently, it is commonly accepted that a SMBH exists at the centre of all large galaxies. [9] Here, a SMBH is defined as a black hole with a mass greater than $10^6 M_\odot$ (one million solar masses). Such an object may be termed an 'AGN' when an associated disc of gaseous matter, surrounds the black hole, whereby matter accretes onto the black hole from the disc. There exist many historical terminologies in the context of AGN, for example: Seyfert galaxies, blazars, quasars, *etc*, these objects are all examples of AGN viewed from differing angles and hence exhibit slightly different spectral features. In the context of this investigation, all such objects will purely be referred to as AGN.

The accretion of matter onto the SMBH results in the emission of large amounts of radiation across the entire range of the electromagnetic spectrum, but particularly in the X-Ray regime, as a result, AGN often out-shine their host galaxy. It is important to note however, that the relative intensity magnitude of the observed radiation emitted by an AGN object is directly related to the rate at which matter flows from the accretion disc into the black hole. Specifically, this process is governed by chaos theory, resulting in AGN exhibiting stochastic behaviour in the observed relative magnitude intensity variations. However, if we assume Keplerian physics to hold true, an AGN that exists within a sub-parsec binary pair would be expected to have an underlying periodicity within the natural stochastic intensity variations. This directly results from perturbations in the accretion flow of matter into the primary black

hole by the orbit of the secondary black hole. As discussed in Graham et al. (2015), the detection of an underlying periodicity is not a fully conclusive identification of a SMBH binary candidate. Periodic intensity variations may arise due to a periodic precession of a possible 'jet' about the axis in a single AGN object, which may arise due to the presence of a warped accretion disc. Although, such situations are rare and the resulting periods are generally an order of magnitude below what we would typically expect for a binary system. Hence, as concluded in Graham et al. (2015), the detection of an underlying periodicity in the time series data for an AGN object, results in this object being a strong SMBH binary candidate.

2 Statistical considerations and Modelling Theory

One of the key considerations in this project is the implementation of a process that adequately models the quasi-periodic and stochastic variations present within the time series data for AGN objects. In order to achieve this, a Continuous-time Auto-Regressive Moving Average (CARMA) modelling technique may be utilized. Presented here, is a basic description to enable a working understanding, with a particular focus on interpretation of the various outputs from the procedure. The finer details regarding the underlying functionality of this statistical tool may be found in Kelly et al. (2014). [13] Further, Bayesian inference for the CARMA model may be applied as one may ascertain the probability distribution of the CARMA process, and therefore allowing for an assessment of periodicity to be performed.

2.1 An Introduction to Bayesian Inference

Bayesian inference is a statistical method enabling estimation of model parameters, uncertainties and calculation of conditional probability. Further, it allows the implementation of a quantitative method of model selection. Specifically, Bayesian inference is defined via Bayes' theorem, given in equation 1 (below).

$$p(\vec{\theta} \mid D, M) = \frac{p(D \mid \vec{\theta}, M)p(\vec{\theta} \mid M)}{p(D \mid M)} \tag{1}$$

Whereby, in equation 1, D, M and $\vec{\theta}$ represent the data acquired, model implemented and the various parameters of the model respectively. The *posterior probability*, which is defined as the probability of the parameter values, given the acquired data and model implemented is given by $p(\vec{\theta} \mid D, M)$. The *likelihood* is defined as the probability for the data given the parameter values in the context of the model and may written mathematically as: $p(D \mid \vec{\theta}, M)$. The prior probability essentially holds any known information regarding the parameter values and is mathematically written as $p(\vec{\theta} \mid M)$. It is important to mention that, in the context of this investigation, flat (or *uniform*) priors were used throughout the entirety of the analysis, as there exists very little knowledge regarding the underlying physical mechanisms governing AGN behaviour. The final parameter in equation 1 is $p(D \mid M)$ and is known as the 'evidence', which is used to normalize the posterior probability and may be calculated through equation 2. For parameter estimation purposes, the evidence may be ignored and samples may be drawn from the unnormalized posterior using standard sampling methods. The evidence however is of extreme significance in quantifying 'model selection', whereby separate models may be ranked against each other through a quantity known as the 'Bayes Factor', which is simply a ratio of the distinct model evidence values. The calculation of such Bayes Factors requires the consideration of Occam's razor which states that a simpler model should be favoured unless a more complicated model significantly outperforms the simpler model. [14]

$$Z = p(D \mid M) = \int p(D \mid \vec{\theta}, M)p(\vec{\theta} \mid M)d\vec{\theta} \tag{2}$$

2.2 CARMA Modelling and Nested Sampling

Presented here, is a basic introduction to the Continuous-time Auto-Regressive Moving Average (CARMA) modelling technique. This is a simplified description of CARMA modelling functionality, for the interested reader, Kelly et al. (2014) and references therein present a more complete explanation of CARMA modelling techniques. [13] In the context of this investigation, the variability of a stochastic and quasi-periodic oscillation may be characterized via a Power Spectral Density (PSD). The PSD encompasses the variability amplitude (or power) per frequency (or within a particular frequency interval). Traditionally, for regularly sampled data, the PSD may be calculated by taking the discrete Fourier Transform of the light curve. However, for cases where the data is not regularly sampled, calculation of the PSD becomes more problematic, especially for stochastic processes. Formation of the PSD allows characterization and assessment of many features, allowing for interpretation of the underlying physical mechanisms. A stochastic differential equation, shown in equation 3 (below) characterizes a zero-mean CARMA(p,q) process $y(t)$. Note that equation 3 highlights that the CARMA process is defined by an autoregressive polynomial term, with order p and moving average polynomial of order q.

$$\frac{d^p y(t)}{dt^p} + \alpha_{p-1}\frac{d^{p-1}y(t)}{dt^{p-1}} + \ldots + \alpha_0 y(t) = \beta_q \frac{d^q \epsilon(t)}{dt^q} + \beta_{q-1}\frac{d^{q-1}\epsilon(t)}{dt^{q-1}} + \ldots + \epsilon(t) \tag{3}$$

The autoregressive polynomial may be calculated through equation 4 and the roots of this polynomial are $r_1, \ldots, r_p$.

$$A(z) = \sum_{k=0}^{p} \alpha_k z^k \tag{4}$$

Here, $\epsilon(t)$ is a zero-mean continuous-time white noise process, with variance σ^2, the parameters $\alpha_0, \ldots, \alpha_p$ and $\beta_1, \ldots, \beta_q$ are the autoregressive and moving average coefficients respectively. In this case, we require that $p > q$ and that the autoregressive polynomial roots have negative real parts in order for the process to remain stationary, whereby the joint probability distribution of the various model parameters does not change when shifted in time. Such a scenario may be inferred, as the period for example, is assumed to remain constant over the temporal baseline for the given dataset, as the separation of a given sub-parsec binary pair is presumed to be unaltered over the temporal baseline. The PSD, may be calculated through equation 5, here f represents the frequency.

$$P(f) = \sigma^2 \frac{|\sum_{j=0}^{q} \beta_j (2\pi i f)^j|^2}{|\sum_{k=0}^{p} \alpha_k (2\pi i f)^k|^2} \tag{5}$$

The autocovariance function defines the covariance of a stochastic process at different times. Whereby, the covariance, is the measure of the join probability of two random variables (expectation value of the product of those variables, minus the product of their means). For the CARMA model, with a time lag τ, the autocovariance may be defined through equation 6. Should, p be odd, as is the case in this investigation (see section 6), the auto-correlation function is a weighted sum of exponentially damped sinusoidal functions. Generally, an odd value of p, allows the existence of one purely real root and complex conjugate pairs for the subsequent roots. Whereby, these complex valued roots indicate oscillatory, exponentially damped behaviour. Note, that as the PSD is given by the Fourier Transform of the autocovariance function, the resulting PSD is a weighted sum of exponential functions, with the centroid of the peaks given by the value of the imaginary part of the root $|\frac{\Im(r_k)}{2\pi}|$ and the widths of the peak are proportional to the real part of the same root $|\Re(r_k)|$.

$$R(\tau) = \sigma^2 \sum_{k=1}^{p} \frac{[\sum_{l=0}^{q} \beta_l r_k^l][\sum_{l=0}^{q} \beta_l (-r_k)^l] \exp(r_k \tau)}{-2\Re(r_k) \prod_{l=1, l\neq k}^{p} (r_l - r_k)(r_l^* + r_k)} \tag{6}$$

The completion of this project involved the implementation of a CARMA(p=3, q=2) process. The particular values for p and q were chosen so that firstly, some of the roots could be complex valued and hence oscillatory behaviour may be observed. One may consider using, for example a CARMA(p=5, q=4) process to add higher order terms to the stochastic differential equation, this added level of complexity

does not significantly add a great deal of value for the extra computational cost, consequently, the CARMA(3,2) model may be deemed most appropriate for use in this context.

If the resulting CARMA(p,q) process is Gaussian in form, calculation of the likelihood may be achieved. Subsequently, maximum-likelihood estimates of the various model parameters may be attained by combining this with a suitable prior. By implementing a state space representation (for details see Kelly et al. (2014)), a Kalman Filter may be utilized in the calculation of the likelihood, resulting in the computational complexity scaling linearly with the number of datapoints, hence, this method is relatively computationally efficient. The Kalman Filter is an algorithm that takes as its input, the prior knowledge regarding the state of the system and the time series measurements. From the prior knowledge state, the Kalman Filter predicts the mean and covariance of the state. This prediction is then compared to the next observation measurement, updating the estimates. This is a recursive process, with the output estimates from the current iteration being the input to the next iteration. Once the mean and covariance of the state have been obtained, it is then possible to calculate the likelihood function, using the Kalman Filter.

Past literature regarding AGN optical intensity variations have often focused on using a Continuous Auto-Regressive [CAR(1)] model, most notably Graham et al. (2014) implemented such a model to simulate AGN intensity variations (see section 3). [2] A CAR(1) model is equivalent to a CARMA(p=1, q=0) model and is often termed a 'Damped Random Walk' (DRW). Kelly et al. (2014) argue that the CAR(1) model is inferior for modelling AGN optical variability compared to the CARMA model employed in this project. The CARMA model allows greater flexibility, as CAR(1) assumes the PSD is a single Lorentzian, with the peak centered at zero. Hence, as the CARMA model adds higher order terms to the characteristic stochastic differential equation, they allow for modelling quasi-periodicities and stochastic variations, which we expect to be present in the case of binary systems. The PSD for a CAR(1) process may be calculated via equation 7, whereby, taking the log of both sides and plotting the PSD gives a power law slope of f^{-2}. Mushotzky et al. (2011), using data from the Kepler telescope reported power law slopes of -2.6 to -3.3, much steeper than simulated by the CAR(1) model. [15] Hence, Kelly et al. (2014) recommend the implementation of the CARMA modelling technique in order to adequately model AGN variability.

$$P(f) = \sigma^2 \frac{1}{\alpha_0^2 + (2\pi f)^2} \tag{7}$$

Here, $\frac{\alpha_0}{2\pi}$ defines the break frequency, at which we see a characteristic 'bend' in the outputted PSD. Also, α_0 is the coefficient of $y(t)$ in equation 3.

Implementation of a nested sampling procedure, allows for calculation of the evidence $'Z'$, which is significant in quantifying model selection, furthermore, posterior samples may be generated as an optional by-product of this procedure. The nested sampling procedure described here is highly condensed and closely follows that of Feroz et al. (2008) [14], for a complete understanding, refer to Skilling (2004) [16]. Brewer et al. (2011) [17] also entails a brief description for the interested reader. A nested sampling procedure enables one to 'climb up' the likelihood function. This is visually displayed for a theoretical two-dimensional problem in figure 1. In essence, nested sampling enables a reduction in parameter-space to one variable (X), transforming the multi-dimensional integral for Z (given in equation 2) to a one-dimensional integral over the prior mass X. The prior mass is defined as $dX = \pi(\vec{\theta})d\vec{\theta}$, where $\vec{\theta}$ are the model parameters and $\pi(\vec{\theta})$ is the *prior*. Hence, Z is now given by equation 8 (below). It is important to mention that calculation of the likelihood may be achieved through implementation of the Kalman Filter.

$$Z = \int_0^1 L(X)dX \tag{8}$$

If we assume X is a decreasing sequence of values, we can approximate this integral as a summation, shown in equation 9, where L_i is the likelihood and w_i is the weight for a value of the prior mass X_i. The weight for the value of the prior mass is given by equation 10. Here, M is denotes the number of prior mass 'segments'.

$$Z = \sum_{i=1}^{M} L_i w_i \tag{9}$$

$$w_i = \frac{1}{2}(X_{i-1} - X_i) \tag{10}$$

The nested sampling procedure may be performed in the following manner: firstly, N live samples are drawn from the full prior. These samples are then sorted in terms of the values of their individual likelihoods, the sample with the smallest likelihood is then replaced by a new sample drawn from the prior with a larger likelihood value, the prior mass is subsequently reduced with each iteration. Termination of the algorithm occurs when the value of the evidence is calculated to within a given accuracy. Through using the calculated Z value and the points generated in the nested sampling process, which are weighted via equation 11, inferences of the posterior parameters may be calculated and the marginalized posterior distribution may be constructed.

$$p_j = \frac{L_j w_j}{Z} \tag{11}$$

Where, $j = 1, 2, \ldots, (M + N)$, here $(M + N)$ represents the total number of sampled points (N - the number of active points, with M - the number of prior mass segments).

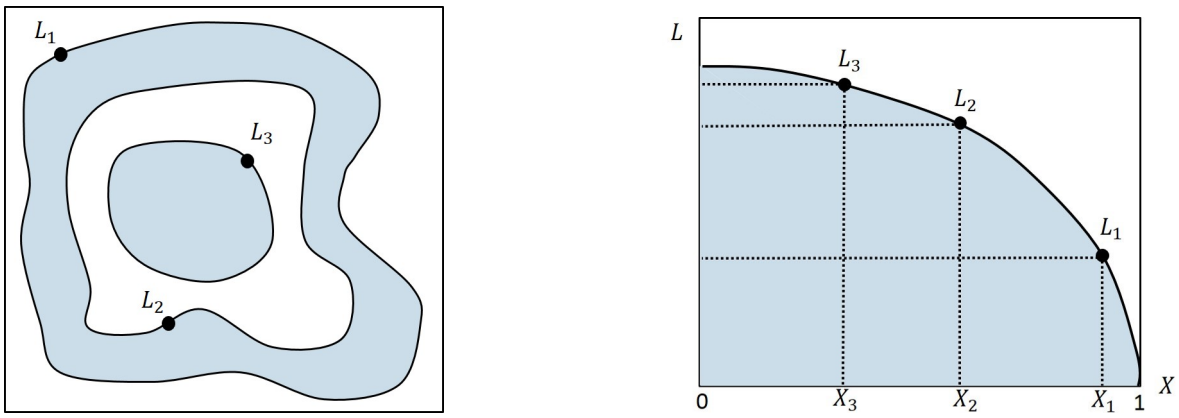

(a) Posterior of a 2-D problem

(b) Likelihood against prior Mass

Figure 1: Theoretical nested sampling, posterior with nested sampling shells, and the likelihood against prior mass

A nested sampling procedure was developed by Dr W. Farr, in Julia language: `http://julialang.org/`. Specifically implementation was performed through the CARMA.jl and Ensemble.jl packages located at: `https://github.com/farr/CARMA.jl` and `https://github.com/farr/Ensemble.jl` respectively. In this investigation, the *nmcmc* variable which sets the number of steps taken before generating a new point to replace the point of low likelihood was set at 128. The number of live points *nlive* was set to 1024. Subsequent code developed by the author and project partner may be found at: `https://github.com/cl-conway/AGN-code`.

3 Discussion of Previously Implemented Methods

This report focuses on evaluating previously implemented methods, specifically regarding the recent claims of SMBH binaries. Of particular interest, is the work by Graham et al. (2015) as this work is both recent and became fairly accepted by the astrophysics community. In this section of the report, a basic description of the methodology and results for the investigation performed by Graham et al. (2015) is provided. The work performed by Graham et al. (2015) employed the Catalina Real-time Transient Survey as the main source for the time series data, further information regarding the use of this data may be found in section 4. Spectroscopically confirmed AGN objects were selected from the million

quasar catalogue (see section 4), along with other sources (namely the Sloan Digital Sky Survey data release 12). The time series data for such objects may then be obtained via the use of the CRTS dataset, notably, a 3 arc-second radius was used in their data retrieval. After the application of pre-processing methods, approximately 250,000 time series data for AGN objects remained and hence could be used in their analysis.

Graham et al. (2015) created a 'mock dataset' by using a CAR(1) process, to simulate the variability for singular AGN objects, whereby no periodic variability in the resulting intensity variations exists. Simultaneously, on the real data, a weighted wavelet Z-transform (WWZ) and auto-correlation function (ACF) methods were implemented, both of which enable detection and estimation of periodic and pseudo-periodic signals in time series data. The details of such methods are discussed by Foster (1996) and McQuillan et al. (2013) respectively. [18] [19] From the implementation of these methods, Graham et al. (2015) developed a selection criteria designed to assess periodicity. The identified objects were then used as 'true positives' in a machine learning algorithm (MLA). The purpose of this MLA was to identify the discriminating hyper-plane across the parameter space that separates the highlighted binary and non-binary candidates from the WWZ and ACF analysis. Hence, by applying the same MLA on both the real and simulated datasets, Graham et al. (2015) hoped to identify periodic binary candidates. Indeed, 111 objects from the real data succeeded, with no objects from the simulated data succeeding, therefore, leading Graham et al. (2015) to conclude that the resulting 111 objects are strong periodic (binary) candidates. In particular, emphasis was placed on object 'PG 1302-102', which, through the analysis performed was the 'best candidate', however the reasoning for this conclusion is unclear.

It is important to mention, that the quoted value for the period of 'PG 1302-102' is 1884 ± 88 days (5.2 years), for this particular object, extra data was added to extend the temporal baseline to approximately 20 years. However, from the implementation of the CRTS data alone, which has a temporal baseline of approximately 9 years, the attained period appears to be 1694 days (see table 2 in [2], where 'PG 1302-102' is named 'BZQJ1305-1033'). The discrepancy between these two values undermines the conclusions of PG 1302-102 exhibiting (quasi-)periodic oscillations. As, one expects the rate of coalescence of the two black holes to be much longer that the temporal baseline for the observations, hence changes in the period during these observations should be negligible. Furthermore, Vaughan et al. (2016) performed extensive analysis on PG 1302-102, concluding that a simple stochastic model was favoured over a sinusoidal process. [6] [2] This investigation aims to apply a CARMA modelling technique in order to compare and quantitatively assess the outputs with the periodic claims for the 111 candidates identified by Graham et al. (2015).

4 Data Utilized

Through the analysis Graham et al. (2015) performed, 111 periodic candidates were identified, out of 250,000 spectroscopically confirmed AGN objects. The data regarding these 111 periodic candidates attained through their analysis may be found by accessing the online version of their publication. In particular, by using the Right Ascension (RA) and Declination (Dec) values stated, one may procure the time series data for these objects from the Catalina Real-time Transient Survey (CRTS) dataset. [5] In order to provide a critical analysis of the claims put forward by Graham et al. (2015) and others, a methodology is to be developed and employed on the periodic candidates selected by Graham et al (2015) and some 'random' AGN objects, which we assume to be non-periodic. Whereby, the data regarding the RA and Dec values for these random objects may be obtained by accessing the 'Million Quasar catalogue' (v4.8b), hence, the resulting time series data for the random objects may then be located in the CRTS database. [20] It is important to note that, efforts were made to attain a larger sample of random AGN objects, such as that employed by Graham et al. (2015), however this was not possible. Hence, in this project, the final analysis may be conducted on time series data for ≈ 300 random objects. Consequently, new periodic candidates could not be suggested through the methodologies implemented in this investigation.

In order to be successful in identifying periodic AGN, one requires access to a LTDS with a long temporal baseline, that routinely observes specific objects. An example of such an LTDS is the Catalina Real-time Transient Survey (CRTS) which was utilized in the completion of this project. [5] To gather data, CRTS employs three separate telescopes: the 0.7 m Catalina Sky Survey Schmidt, the 1.5 m Mount Lemmon Survey and the 0.5 m Siding Springs Survey Schmidt. CRTS has approximately 9 years of photometric

data, spanning a 33,000 square degree area. From these telescopes, the CRTS team have obtained the time series data for approximately 500 million astronomical objects in the range: $-75° < \text{Dec} < 70°$.

4.1 Data Acquisition and Processing

It was deemed necessary to implement a pre-processing method which selected suitable random objects for the analysis. Firstly, in order to ensure that the random objects examined were indeed AGN, only those objects with a quasar percentage greater than 95% from the 'Million Quasar catalogue' were considered. The quasar percentage value is based on the photometric data for that object. Initially, 5000 random objects were selected from the Million Quasar database, it is important to note that similarly to Graham et al. (2015), a 3 arc-second radius was applied to the co-ordinates found from the 'Million Quasar catalogue'. Furthermore, all selected objects were required to have at least 50 data points across the entire CRTS temporal baseline, in order to reduce statistical systematic effects.

In order for an appropriate comparison to be made, the selected random AGN objects should be sampled to a similar quality to the candidates identified by Graham et al. (2015). Hence, calculation of the mean and standard deviation for the size of the error bars across all Graham et al. candidates was undertaken, with an attained value of: 0.12 ± 0.04. Subsequently, random objects whom have an error bar mean greater than 1 standard deviation above the Graham candidates error bar mean are thus rejected. A final consideration in the development of the selection criteria is that of data which is sampled very unevenly in time. The inclusion of such data may result in problems with the modelling techniques implemented. In order to quantify this criterion, the ratio of the median time value to the overall time range for the data was calculated, those objects for whom this value lay outside the range 0.3 - 0.7 were subsequently rejected.

To maximize the effectiveness of the modelling techniques, the implementation of a method to remove outliers is required. Graham et al. (2015) also recognized the need to appropriately remove significant outliers, whereby the mechanism they applied involved a complex process with the use of a three-point median filter, as explained by Palanque-Delabrouille et al. (2011). [21] In the context of this project, such a complex routine is not necessary, instead a basic sigma-clipping routine may be executed, with the σ-level set as 5. Overall, 312, of the original 5000 randomly selected objects are present on the CRTS database and survived the pre-processing. Notably, 17 of the Graham et al. (2015) periodic candidates did have slightly larger error bars than the criterion, rejection of these objects was not performed in order to have a complete and thorough comparison of the random objects with the full periodic candidate dataset. A full summary regarding object rejection is detailed in table 1.

Selection Criteria Description	Random Objects	Graham Objects
Objects Submitted to CRTS	5000	111
No. Objects on CRTS	3491	111
No. Objects greater than 50 obs.	2352	111
No. Objects with suitable error bars	321	94
No. Objects without scewed time data	312	111
Sigma Clipping % of data removed	2.79%	0.84%
Object Survival Percentage	8.94%	N/A

Table 1: Object survival at each stage of the selection criteria

5 Preliminary Investigations

Before implementation of the CARMA modelling techniques described in section 2.2, preliminary investigations were performed, with a specific focus on the best candidate in the analysis performed by Graham et al. (2015), 'PG 1302-102'. Initially, the time series data for object 'PG 1302-102' was fitted to a Lomb-Scargle (L-S) periodogram. Whereby, a generalized L-S model may be described through equation 12, here ω is a given frequency, with Period P ($P = \frac{2\pi}{\omega}$). The in-depth functionality of the L-S modelling technique is described in detail by Zechmeister and Kürster (2009). [22] The L-S model enables one to fit a sinusoid to irregularly sampled data, by optimizing this fit, a value for the period of

object 'PG 1302-102' may be obtained. In order to simulate Gaussian noise, the individual datapoints may be distributed across the error bars in a Gaussian manner, using the original datapoint as the mean and the error bars as the standard deviation. Performing this process for 1000 iterations, obtaining a value for the period in each case. It is important to mention that implementation of the L-S periodogram was performed via the use of the *gatspy* python package (see Vanderplas and Ivezić). [23]

$$\phi(t) = A\sin(\omega t) + B\cos(\omega t) + C \tag{12}$$

A further technique which may be employed in order to obtain the period for 'PG 1302-102', is a Markov Chain Monte Carlo (MCMC) simulation. A complete description regarding MCMC methods may be found in Mackey et al. (2013). [24] MCMC methods enable the use of a Bayesian approach to statistics as described in section 2.1. In particular, MCMC enables the efficient marginalization over nuisance parameters, such as the phase and amplitude, resulting in calculation of the *marginalized probability function*. In this investigation, the *emcee* sampler method was utilized, thereby allowing draws from the posterior probability density to take place, with calculation of the relevant *likelihood* and *prior*. [24] The 'Markov Chain' element ensures that the future state of the system is only dependent on the systems current state. Once the draws of the posterior probability density have been performed, the probability distribution for the attained period values may be plotted, this is shown in figure 2a, with an equivalent plot for the L-S modelling technique. The fit of the outputted MCMC and L-S models to the light curve for 'PG 1302-102' is shown in figure 2b.

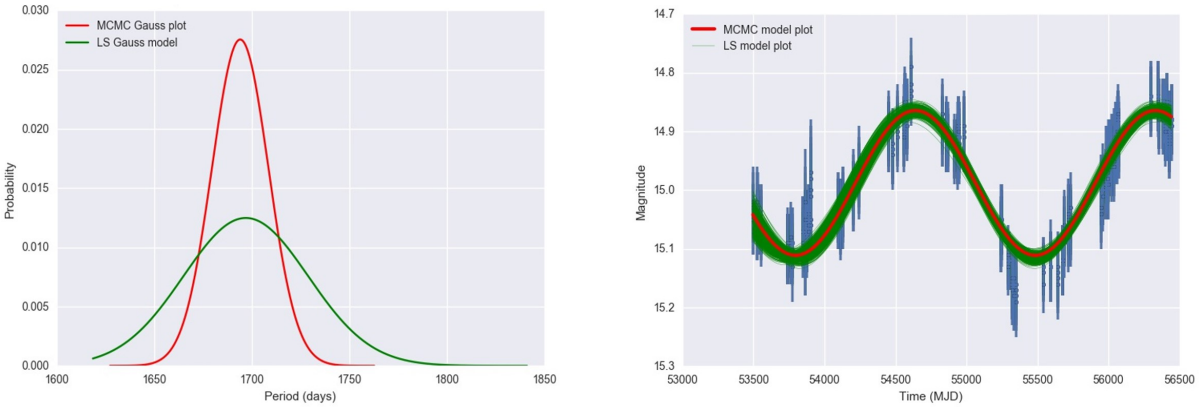

(a) Gaussian fit, period values

(b) Light Curve

Figure 2: LS and MCMC model outputs for object PG 1302-102

Through the analysis performed by Graham et al. (2015) a period value of 1884 ± 88 days (or 5.16 ± 0.24 years) was found for 'PG 1302-102'. [1] However, a different period value for the same object was quoted by Graham et al. (2015) [2] with a value of 1694 days (or 4.64 years), with no stated error values. Vaughan et al. (2016) performed an extensive analysis on object 'PG 1302-102', by using a least squares fit, similar to the L-S fitting technique applied in this investigation, a period of 4.65 ± 0.06 years was attained through their analysis. [6] The preliminary results from this investigation found period values of 4.65 ± 0.08 and 4.64 ± 0.04 years for the L-S and MCMC techniques respectively. Therefore, the results from this investigation are in good agreement with the analysis performed by Vaughan et al. (2016), furthermore, they also strongly agree with the original value attained by Graham et al. (2015). [2] However, these values are in stark contrast to the values quoted by Graham et al. (2015), notably 1884 ± 88 days or 5.2 years. [1] This discrepancy in attained period values significantly weakens the claim regarding 'PG 1302-102' having (quasi-)periodic oscillations.

6 Main Results

A CARMA(3,2) model as descrided in section 2.2 was applied to the 111 identified Graham candidates and the 312 randomly selected (presumed non-binary) AGN objects, via the use of a nested sampling procedure. It is hoped that by comparing the outputs of the two datasets from the CARMA modelling

technique, a quantitative evaluation may be performed which allows assessment of the periodicity claims regarding the Graham candidates. It is important to mention that a maximum frequency value was set at 1 day in order to remove the high frequency noise present in the modelling. This is a reasonable upper limit for the frequency, the derivation for this is located in section A.1, in the Appendix. Further, a lower limit was set by the temporal baseline of the relevant objects data.

6.1 PSD Outputs

As stated in section 2.2 a peak in the outputted power spectral density (PSD) is an indicative feature of an underlying oscillation, whereby the peak occurs at a frequency which corresponds to the period of the detected oscillation. However, it is important to show explicitly that this is the case. In order to achieve this, a simulated dataset may be created which uses the times at which the data was taken for the given objects, but enforces a sinusoidal variation of the magnitude values, with the error bars remaining unchanged. This data may then be fed through the CARMA(3,2) model, sampling over the posterior to form the PSD, which may subsequently be compared to the PSD for the real data of the same object. This process was applied to all the identified periodic candidates by Graham et al. (2015), with the period value inserted into the sinusoidal process being the period value acquired through the analysis performed by Graham et al. (2015). Figure 3 shows the PSD for the real and simulated data, for object "SBS 0920+590". Here, it may be seen that a clear, sharp peak is present in the PSD for the simulated data, however, for this object no clear peak is present in the PSD for the real data. Hence, this explicitly shows that a peak in the PSD is an indicative feature of an underlying sinusoidal behaviour.

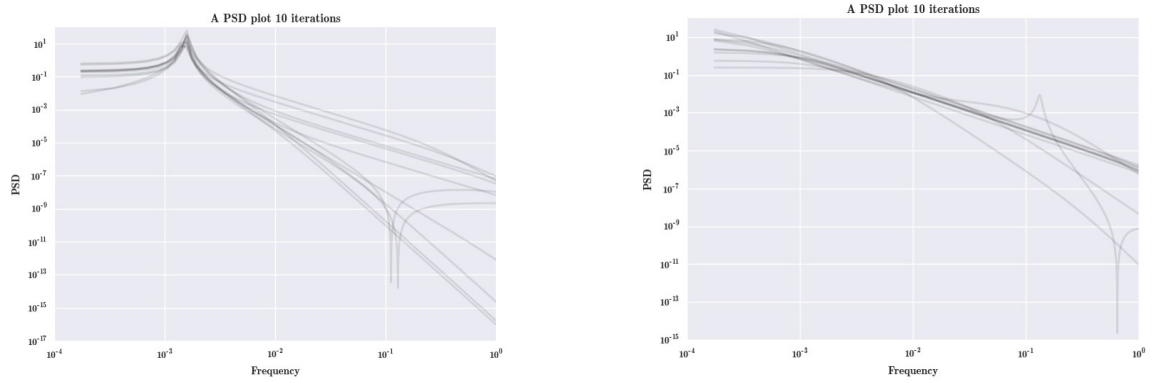

(a) Simulated Data

(b) Real Data

Figure 3: Generated PSDs from CARMA for Graham object "SBS 0920+590"

The PSD for the real data of the best performing Graham periodic candidate "SDSS J144755.57+100040.0", as quantified through this investigation via the oscillatory statistic (see section 6.2) is shown in figure 4 , along with the PSD for the real data of "PG 1302-102", the best periodic candidate through the analysis performed by Graham et al. (2015).

Comparison of the two PSD plots in figure 4 shows a clear peak in the best performing object through the CARMA modelling technique, in stark contrast to "PG 1302-102" which, through this analysis performs extremely poorly with no clear identifiable peak present in the PSD. It is important to mention, that through the CARMA(3,2) fitting procedure, the ν values were calculated. These values represent the overestimation of the data error bars by CRTS and may be found through examination of the intensity fluctuations on very short (less than 20 day) timescales. The majority of the objects in this investigation returned ν values of roughly 0.2 - 1.5, with the vast majority being clustered in the range 0.6 - 1.0. Generally, no significant difference exists between the ν values for the random AGN objects and the Graham et al. periodic candidates. The ν value for object 'PG 1302-102' obtained through this experiment was 0.2, a value which is consistent with that found by Vaughan et al. (2016). Histograms of the probability density for the ν values are located in figure 5.

The gradient values observed in the (log-log) PSD for AGN objects observed (through Kepler data) by Mushotzky at al. (2011) were ≈ -2.6 to -3.3. [15] Thus highlighting that the CAR(1) process is not sufficient to describe AGN variability as discussed in section 2.2. In this investigation, the slope of the

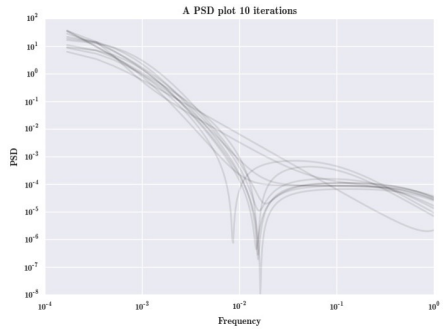

(a) PSD for "PG 1302-102"

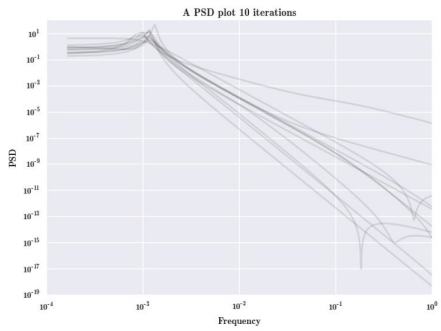

(b) PSD for "SDSS J144755.57+100040.0"

Figure 4: PSDs for best Graham candidate in this analysis and "PG 1302-102"

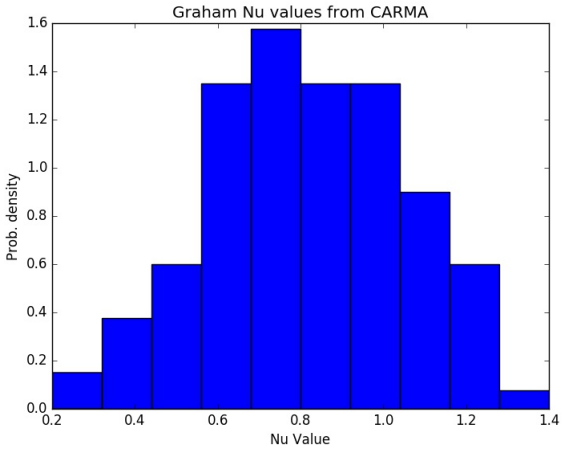

(a) Graham et al. periodic candidates ν values

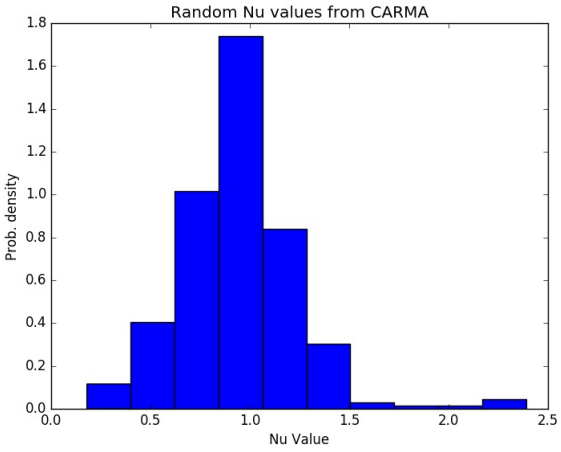

(b) Random Objects ν values

Figure 5: ν Values for the Random and Graham et al. Objects

PSD is calculated at a frequency of $f = 0.01$, this value was chosen qualitatively, as for the majority of objects examined, a present peak in the PSD occurs at lower corresponding frequencies and there is a relatively small amount of noise at this value. The attained gradient values were plotted as histograms, shown in figure 6.

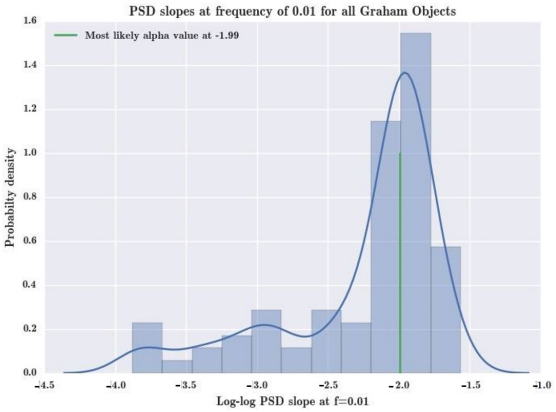

(a) Graham et al. candidates PSD Gradient values

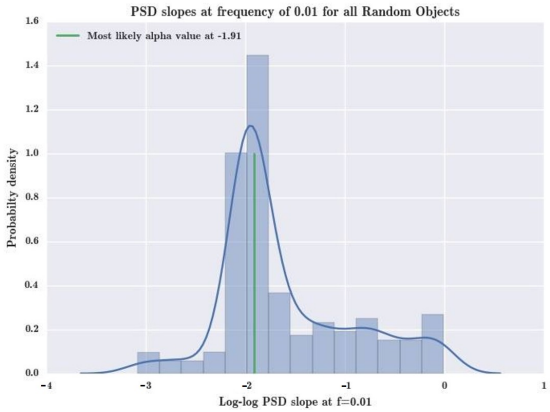

(b) Random Objects PSD Gradient values

Figure 6: PSD Gradient values at $f = 0.01$

As shown in figure 6, the spread of the gradient values is much larger than previously thought, with

values extending over the range ≈ -1 to -4, larger than those observed by Mushotzky et al. (2016). [15] This is yet further evidence which suggests that the CAR(1) process is not adequate to model AGN variability and therefore, the utilization of CARMA models is appropriate in this context.

6.2 Oscillatory Statistic

Visual displays of the PSD provide a qualitative measure of periodicity for individual AGN objects. Quantification of this may be achieved by defining an 'oscillatory statistic', whereby the oscillatory statistic is defined as the fraction of posterior samples that contain non-zero imaginary parts in the complex roots for the autoregressive polynomial discussed in section 2.2. From the value of the imaginary part of the complex root, one may infer the period of the oscillations through equation 13, where T is the period and $\Im(r_k)$ is the imaginary part of the complex root. For the CARMA(3,2) model $k \neq 1$ as this represents the purely real root. Computation of the oscillatory statistic and associated period values were performed in this experiment on all (random and Graham et al. periodic candidate) objects.

$$T = \frac{2\pi}{|\Im(r_k)|} \tag{13}$$

Objects that exhibit stronger periodic behaviour have a higher oscillatory statistic, as a greater number of roots within the posterior samples contain non-zero imaginary parts. Hence, by ordering the objects in terms of this value, a 'gains chart' may be formed which depicts the relative distribution of the Graham et al. (2015) periodic candidates amongst the entire object population, this is depicted by the blue line in figure 7. In figure 7, the green line is known as the 'random line' and illustrates the expected distribution of Graham et al. (2015) periodic candidates for an unsorted dataset. It is important to highlight, that if the Graham candidates had high oscillatory statistics (and therefore indicated high likelihoods of periodicity), one would expect the blue curve in figure 7 to exist in the top left hand corner of the plot. However, upon inspection, it may be concluded that the distribution of Graham candidates tracks the 'random' line fairly closely, indicating therefore that the periodic candidates identified by Graham et al. (2015) perform poorly in this 'oscillatory statistic' criterion. This analysis therefore suggests, that as a population, the periodic candidates identified by Graham et al. (2015) do not show significantly more periodic behaviour than random (singular) AGN objects. Subsequently, this analysis directly contradicts the SMBH binary claims put forward by Graham et al. (2015).

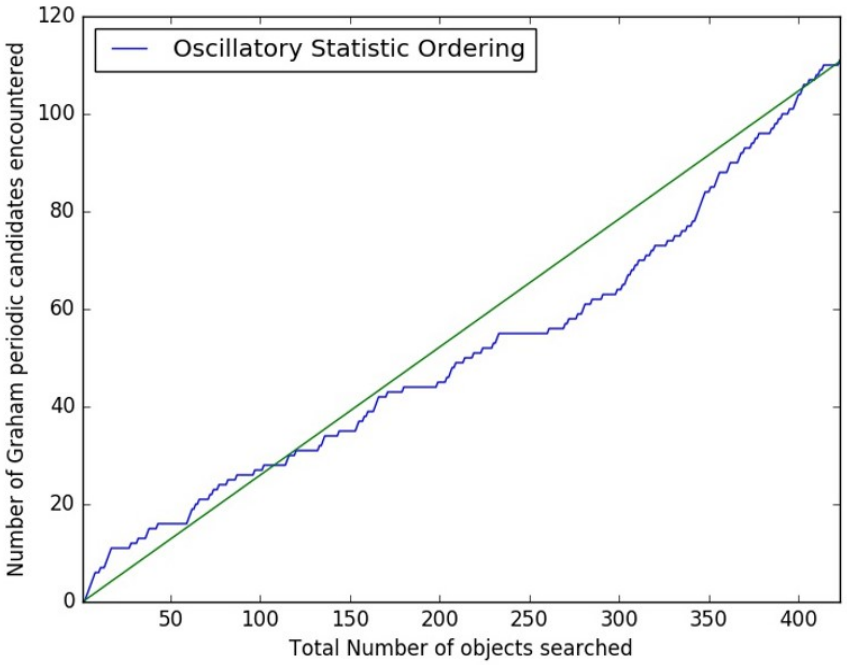

Figure 7: Gains Chart, quantifying the Oscillatory statistic for all 312 'random' and 111 'periodic candidate' objects

Generally, an object with an oscillatory statistic of less than 0.5 may be considered as non-oscillatory. Therefore, for this particular dataset, 28 out of the total 423 objects show oscillatory behaviour as quantified by the oscillatory statistic. Table 2 shows the 10 objects with the highest (best) oscillatory statistic, alongside the period attained through this analysis, object PG 1302-102 is also included for comparative purposes. Note that the 'Type' in table 2 represents 'R' for a random object and 'G' for a periodic candidate identified by Graham et al. (2015). Furthermore, the 'G Period' is the period value attained by Graham et al. (2015) for that particular object.

Ranking	Object Name	Type	Osc. Stat	Period(days)	G Period(days)
1	PGC1023662	R	1	$360.66^{+9.07}_{-9.15}$	N/A
2	SDSS J000217.97-022437.9	R	0.999	$353.76^{+11.24}_{-11.3}$	N/A
3	SDSS J144755.57+100040.0	G	0.949	$849.42^{+100.76}_{-83.65}$	862
4	SDSS J142301.96+101500.1	G	0.893	$1197.76^{+204.13}_{-150.61}$	1234
5	SDSS J224829.47+144418.0	G	0.843	$1282.2^{+249.58}_{-150.22}$	1219
6	HS 0423+0658	G	0.839	$1069.99^{+235.82}_{-178.37}$	1123
7	SDSS J221016.97+122213.9	G	0.838	$1389.1^{+383.69}_{-193.97}$	1333
8	SDSS J080237.60+340446.3	G	0.776	$1556.88^{+309.2}_{-202.33}$	1428
9	SDSS J000308.10+314816.1	R	0.774	$48.28^{+2.63}_{-6.49}$	N/A
10	SDSS J000544.19+171153.1	R	0.692	$1504.72^{+418.15}_{-255.66}$	N/A
409	PG 1302-102	G	0.083	$1398.04^{+917.7}_{-1395.97}$	1694

Table 2: Oscillatory Statistic (Osc. Stat), top 10 objects and PG 1302-102

From table 2, the top two performing objects in the oscillatory statistic criterion are 'random' objects. This is unexpected as the random objects may be assumed as singular (non-binary) AGN, thus an underlying period should not be seen. However, the attained period values for these two objects are suspiciously close to 1 year, hence suggesting that a calibration error may exist for these two objects in the CRTS database. Of these top 10 objects, 6 are Graham periodic candidates, with 5 of these having oscillatory statistic values greater than 0.8, indicating a high chance of underlying oscillatory behaviour. The period values attained for all these objects, coincide with the period values attained by Graham et al. (2015). However, it must be noted that the errors on the periods acquired through the analysis performed in this investigation are large, mostly due the small time span over which the data has been taken. Therefore, it is possible to argue that these results support the analysis performed by Graham et al. (2015), however, only 12 of the 111 periodic candidates identified by Graham et al. (2015) have an oscillatory statistic greater than 0.5 (compared to 16 random objects) and only 5 of these periodic candidates show strong oscillatory behaviour (oscillatory statistic greater than 0.8). Furthermore, the best performing candidate from the analysis performed by Graham et al. (2015), 'PG 1302-102', ranked 409^{th} out of 423 objects, with an oscillatory statistic of 0.083. The extremely poor performance of this object in the oscillatory statistic criterion directly questions the validity of the analysis and hence conclusions regarding the detected oscillations in all 111 Graham periodic candidates.

6.3 Best Periodic Candidate

Excluding the two random objects found through the CARMA analysis, whose relatively strong performance may be attributed to a CRTS calibration error (see section 6.1), the best performing object, as quantified by the oscillatory statistic is: "SDSS J144755.57+100040.0". Presented here, is further analysis on this object with regard to the quality factor of the oscillations and also a depicted fit of the CARMA process to the data. The quality factor may be determined via equation 14 (below):

$$Q = \frac{1}{2\pi}\left|\frac{\Im(r_k)}{\Re(r_k)}\right| \tag{14}$$

Whereby, Q, $\Im(r_k)$ and $\Re(r_k)$ represent the Quality factor, imaginary part of the autoregressive polynomial root and the real part of the same root respectively. This is equivalent to the centroid over the FWHM of the Lorentzian in the PSD corresponding to the complex root. Once again, this quality factor

was calculated only for those roots with a non-zero imaginary part of the root within the reasonable frequency range, detailed in section 6.1. The quality factor is defined as the number of cycles over which the oscillating signal decays by a factor of $\frac{1}{e} \approx 0.37$. Generally, a value of $Q > 0.5$ gives an underdamped system whereby the oscillations may be appropriately observed. Hence, if the oscillations are at a low quality factor, the oscillatory behaviour may in fact not be meaningful, hence by examining the quality factor for the best performing object in this analysis, one may infer whether the detected oscillations are indicative of a true periodicity (see Kelly et al. [2014] for details). [13] The obtained value for the Quality Factor for this object is: $Q = 1.14^{+1.14}_{-0.61}$, and the probability distribution for the Quality Factor is shown in figure 8. From figure 8, it may be concluded that this object is likely be an underdamped system ($Q > 0.5$), therefore, the underlying (quasi-)periodicity is likely to have a meaningful origin. It is important to mention that the physical origin of the damping is not fully understood, as the underlying physics of an AGN binray system are too complex to be fully modelled in detail.

The CARMA model may be fitted to the original data for the objects. Figure 9 shows the CARMA fits to the data for the best performing object from this analysis (as quantified by the 'oscillatory statistic'), compared to object 'PG 1302-102'. As highlighted by Vaughan et al. (2016), the light curve for 'PG 1302-102' qualitatively appears sinusoidal in nature, however, the large change in amplitude along with the very few number of observed cycles result in an extremely poor fit by the CARMA model. Conversely, the Graham periodic candidate with the largest 'oscillatory statistic', produces a well-defined CARMA fit.

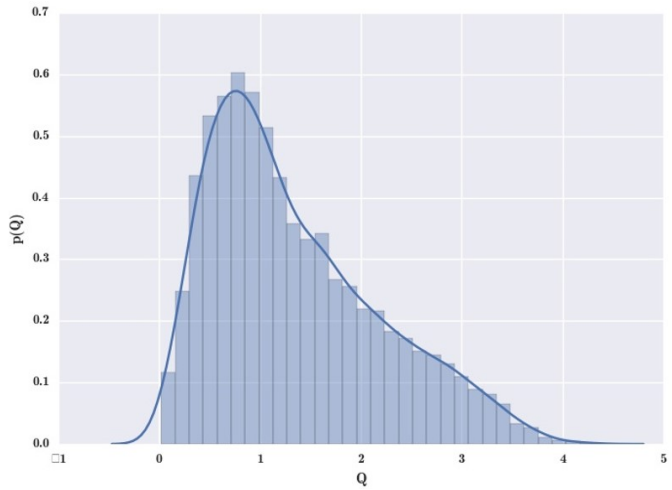

Figure 8: Quality Factor distribution for best performing candidate

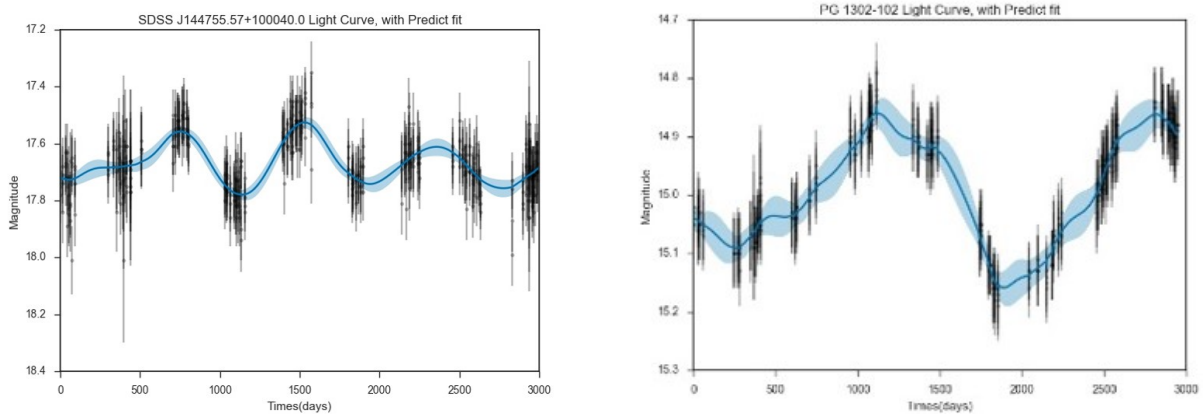

(a) Graham candidate highest Osc. Stat.

(b) Object 'PG 1302-102'

Figure 9: CARMA model fits to the original data

6.4 Bayes Factor

Objects with high oscillatory factors are indicative of having underlying periodicity. However, stochastic processes may exhibit sinusoidal variations, therefore, in order to identify truly sinusoidal processes, one must compare the relative performance by the CAR(1) and CARMA(3,2) models. This may be done through a quantity known as the 'Bayes Factor', which is calculated as the ratio of the evidences for the two relevant models, as shown in equation 15. Truly periodic objects are expected to have both a high oscillatory statistic and a high Bayes factor (showing significant preference towards the CARMA(3,2) model over the CAR(1) process). The previously discussed, best performing Graham et al. (2015) periodic candidate, as quantified by the oscillatory statistic: "SDSS J144755.57+100040.0", has a calculated Bayes Factor of 57.4, showing a 'very strong' preference for the CARMA(3,2) model. Hence enforcing the conclusion that this object appears to contain an underlying periodicity in the intensity variations. Importantly, the use of the Harold Jeffrey's' scale allows for a qualitative assessment of the relative strength of the Bayes Factor. [25] Table 3 details the percentage splits of the relevant datasets across the Harold Jeffrey's ranking scale.

$$K = \frac{p(D|M_1)}{p(D|M_2)} \tag{15}$$

In equation 15, K represents the Bayes Factor, $p(D|M_x)$ represents the evidence value for model x where $x = 1, 2$ in equation 15. From table 3 it can be seen that the CARMA(3,2) model is more favoured by the Graham objects than the random objects. This may arise due to Graham objects having been hand-picked based on specific features, therefore, these objects exhibit greater complexity which may be more appropriately modelled by a CARMA(3,2) than CAR(1) process. 'Favouring' here is quantified through the Bayes Factor being larger than $10^{1/2} \approx 3.16$, hence it has a 'substantial favouring' or greater. Of the 28 objects with an oscillatory statistic greater than 0.5, 16 had Bayes' Factor rankings of 'substantial' or higher, with 11 of these 16 objects being periodic candidates identified by Graham et al. (2015). Hence, as one would expect, those showing oscillatory behaviour tend to have larger relative Bayes Factors.

Bayes Factor Interpretation	**Random Objects (%)**	**Graham Objects (%)**
Decisive	2.88	6.31
Very Strong	0.96	4.50
Strong	0.96	2.70
Substantial	4.17	10.81
CARMA Favoured	8.97	24.32

Table 3: Bayes Factor interpretations, using Harold Jeffrey's scale

7 Conclusion

The detection of an underlying periodicity in the intensity variations from optical time series data for AGN objects is an effective method for identifying SMBH binary candidates. The results from this investigation highlight that the periodic candidates identified by Graham et al. (2015) are quantitatively no more periodic than a set of random (presumed non-binary) AGN objects. Importantly, the detection of two random objects ("PGC1023662" and "SDSSJ000217.97-022437.9") with extremely strong periodic oscillations on timescales corresponding to ≈ 1 year highlights the existence of a calibration issue existing in the CRTS time series data for those two objects. Some Graham et al. periodic candidates, in particular: "SDSS J144755.57+100040.0" showed strong evidence of oscillatory behaviour through both a high oscillatory statistic and Bayes Factor, with an attained period value of $849.42^{+100.76}_{-83.65}$ days, this value agrees with the value attained by Graham et al. (2015): 862 days. Further, the measured Quality Factor for the oscillations of this object was calculated to be: $Q = 1.14^{+1.14}_{-0.61}$, emphasizing that the observed oscillations are 'underdamped', consequently enabling them to be observed.

In contrast, "PG 1302-102", the best candidate from the analysis implemented by Graham et al. (2015), performed extremely poorly in this analysis, which directly questions the validity of the subsequent periodicity claims made. A key point made by Vaughan et al. (2016) is that the detected oscillations of "PG 1302-102" are only observed for 1.5 cycles, whereby they found that sinusoidal variations were difficult to detect for a temporal baseline that was fewer than 2 cycles. For object "SDSS J144755.57+100040.0", the oscillations are detected for 3.5 cycles, strengthening the argument that this object exhibits periodic behaviour, however a definitive periodicity is likely to not be attained until oscillations are detected for approximately 5 cycles. The significant preference of the Graham et al. periodic candidates over the random objects towards the CARMA process indicates that these selected candidates have complex additional features which may not be fully captured through a CAR(1) process. However, the results of this investigation highlight that these features are not periodic behaviour, indeed there exact nature is not fully understood. Further evidence for the favourability of CARMA over CAR(1) processes in modelling AGN variability is the PSD gradient values attained. Specifically, the spread of the gradient values from ≈ -1 to -4 is further evidence that a CAR(1) process, which assumes the PSD gradient is ≈ -2, may not be an appropriate method for characterizing AGN variability.

In this investigation, the full CRTS dataset could not be attained and hence, new SMBH binary candidates could not be identified through the application of a CARMA modelling technique. The relative success of this project highlights that future studies may successfully identify SMBH binary candidates via the application of a CARMA modelling process on a large dataset of AGN time series data (≈100,000 objects). Furthermore, other SMBH binary claims in the literature such as Zheng et al. (2016) may be assessed through a similar method adopted here. [26]

8 Acknowledgments

The author of this report would like to thank Dr Will Farr, for his assistance, advice and supervision. Also, thank you to my project partner Christopher Conway, whom was patient and a pleasure to work with. My thanks to the *University of Birmingham* staff for the provision of facilities and education in order to allow this investigation to take place. Finally, an extension of thanks to the CRTS data acquisition team whom are supported by the National Science Foundation under grants AST-0909182 and AST-1313422. This work made use of the Million Quasar Catalogue and data provided by Graham et al. (2015) via their online publication.

References

[1] M. J. Graham, S. G. Djorgovski, D. Stern, A. J. Drake, A. A. Mahabal, C. Donalek, E. Glikman, S. Larson, and E. Christensen, "A possible close supermassive black-hole binary in a quasar with optical periodicity," *Nature (Nature Publishing Group, a division of Macmillan Publishers Limited. All Rights Reserved.)*, vol. 518 Issue 7537, pp. 74–76, 2015. Last Accessed: 2nd Nov. 2016.

[2] M. J. Graham, S. G. Djorgovski, D. Stern, A. J. Drake, A. A. Mahabal, C. Donalek, E. Glikman, S. Larson, and E. Christensen, "A systematic search for close supermassive black hole binaries in the catalina real-time transient survey," *Monthly Notices of the Royal Astronomical Society*, vol. 453, no. 2, pp. 1562–1576, 2015.

[3] B. P. Abbott *et al.*, "Ligo: the laser interferometer gravitational-wave observatory," *Reports on Progress in Physics*, vol. 72, no. 7, p. 076901, 2009.

[4] M. Preto, I. Berentzen, P. Berczik, and R. Spurzem, "Fast Coalescence of Massive Black Hole Binaries from Mergers of Galactic Nuclei: Implications for Low-frequency Gravitational-wave Astrophysics," *arXiv*, vol. 732, p. L26, 2011.

[5] A. Drake *et al.*, "First results from the catalina real-time transient survey," *ApJ*, vol. 696, no. 870, 2009.

[6] S. Vaughan, P. Uttley, A. G. Markowitz, D. Huppenkothen, M. J. Middleton, W. N. Alston, J. D. Scargle, and W. M. Farr, "False periodicities in quasar time-domain surveys," *Monthly Notices of the Royal Astronomical Society*, vol. 461, no. 3, pp. 3145–3152, 2016.

[7] Liu, Y., Jiang, D. R., Shen, Z.-Q., and Karouzos, M., "A kinematic study of the compact jet in quasar b31633+382," *AA*, vol. 522, p. A5, 2010.

[8] M. G. Haehnelt and G. Kauffmann, "Multiple supermassive black holes in galactic bulges," *MNRAS*, vol. 336, Nov. 2002.

[9] S. Komossa and J. Zensus, "Compact object mergers: observations of supermassive binary black holes and stellar tidal disruption events," *Proceedings of the International Astronomical Union*, vol. 10, 2014.

[10] S. Komossa, V. Burwitz, G. Hasinger, P. Predehl, J. S. Kaastra, and Y. Ikebe, "Discovery of a binary active galactic nucleus in the ultraluminous infrared galaxy ngc 6240 using chandra," *The Astrophysical Journal Letters*, vol. 582, no. 1, p. L15, 2003.

[11] M. Milosavljevic and D. Merritt, "The Final parsec problem," *AIP Conf. Proc.*, vol. 686, pp. 201–210, 2003. [,201(2002)].

[12] M. Enoki, K. T. Inoue, M. Nagashima, and N. Sugiyama, "Gravitational waves from supermassive black hole coalescence in a hierarchical galaxy formation model," *The Astrophysical Journal*, vol. 615, no. 1, p. 19, 2004.

[13] B. C. Kelly, A. C. Becker, M. Sobolewska, A. Siemiginowska, and P. Uttley, "Flexible and scalable methods for quantifying stochastic variability in the era of massive time-domain astronomical data sets," *The Astrophysical Journal*, vol. 788, no. 1, p. 33, 2014.

[14] F. Feroz, M. P. Hobson, and M. Bridges, "Multinest: an efficient and robust bayesian inference tool for cosmology and particle physics," *Monthly Notices of the Royal Astronomical Society*, vol. 398, no. 4, p. 1601, 2009.

[15] R. F. Mushotzky, R. Edelson, W. Baumgartner, and P. Gandhi, "Kepler Observations of Rapid Optical Variability in Active Galactic Nuclei," *ApJ*, vol. 743, p. L12, 2011.

[16] J. Skilling, "Nested sampling for general bayesian computation," *Bayesian Anal.*, vol. 1, pp. 833–859, 12 2006.

[17] B. J. Brewer, L. B. Pártay, and G. Csányi, "Diffusive nested sampling," *Statistics and Computing*, vol. 21, no. 4, pp. 649–656, 2011.

[18] G. Foster, "Wavelets for period analysis of unevenly sampled time series," *Astronomical Journal*, vol. 112, p. 1709, Oct. 1996.

[19] A. McQuillan, S. Aigrain, and T. Mazeh, "Measuring the rotation period distribution of field m dwarfs with kepler," *Monthly Notices of the Royal Astronomical Society*, vol. 432, no. 2, p. 1203, 2013.

[20] E. W. Flesch, "The Half Million Quasars (HMQ) Catalogue," *Publ. Astron. Soc. Austral.*, vol. 32, p. 10, 2015.

[21] D. Palanque *et al.*, "Variability selected high-redshift quasars on SDSS Stripe 82," *AAP*, vol. 530, p. A122, June 2011.

[22] M. Zechmeister and M. Kürster, "The generalised Lomb-Scargle periodogram. A new formalism for the floating-mean and Keplerian periodograms," *AAP*, vol. 496, pp. 577–584, Mar. 2009.

[23] J. T. VanderPlas and Ž. Ivezić, "Periodograms for Multiband Astronomical Time Series," *APJ*, vol. 812, p. 18, Oct. 2015.

[24] D. Foreman-Mackey, D. W. Hogg, D. Lang, and J. Goodman, "emcee: The mcmc hammer," *PASP*, vol. 125, pp. 306–312, 2013.

[25] H. Jeffreys, *The Theory of Probability*. Oxford University Press, 3rd ed., 1961.
Pages 432.

[26] Z.-Y. Zheng, N. R. Butler, Y. Shen, L. Jiang, J.-X. Wang, X. Chen, and J. Cuadra, "Sdss j0159+0105: A radio-quiet quasar with a centi-parsec supermassive black hole binary candidate," *The Astrophysical Journal*, vol. 827, no. 1, p. 56, 2016.

Appendix A

A.1 Upper Limit on Frequency Derivation

Here, a derivation of the upper limit on the frequency for a binary black hole system is given and shown to be of the order of 1 day.

Firstly, we assume that the black holes in the supposed binary system are of equal mass $M = 10^8 M_\odot$, where $M_\odot$ represents 1 solar mass. Secondly, we assume that the separation of this binary pair is at twice the Schwarschild radius (the minimum possible separation for the black holes in a binary system). Finally, we assume Kepler's laws hold true in this system.

From these assumptions, the separation r of the two black holes and the period of the oscillation T are given by:

$$r = \frac{4GM}{c^2}$$

$$T = \sqrt{\frac{4\pi^2 r^3}{2GM}}$$

Here, G is the Gravitational constant and c is the speed of light. Solving this gives:

$$T = \frac{16\pi GM}{\sqrt{2}c^3}$$

Substituting the values of $G = 6.67 \times 10^{-11}\ \mathrm{m^3\,kg^{-1}\,s^{-2}}$ and $c = 3 \times 10^8\ \mathrm{m\,s^{-1}}$ obtains a value for T of: $T = 16.77 \times 10^3$ s or $T = 0.194$ days

As $f = \frac{1}{T}$, an upper limit on the frequency is $\approx 5\ \mathrm{days}^{-1}$. Therefore, an upper limit of $1\ \mathrm{days}^{-1}$ on the frequency is not unreasonable.

A.2 Random Object Data

The Right Ascension and Declination values for the Random Objects used in this investigation are given in table 4 (below):

ID	RA	Dec
SDSSJ000002.92-051940.0	0.0121818	-5.3277779
SDSSJ000003.18-074105.9	0.0132911	-7.6849799
SDSSJ000003.29-025440.1	0.013746	-2.9111321
SDSSJ000008.48+125033.5	0.0353482	12.8426352
LBQS2357-0014	0.049839	0.040365
SDSSJ000013.35+330154.0	0.0556536	33.0316658
SDSSJ000015.47+005246.8	0.064497	0.879677
SDSSJ000016.17-030604.5	0.0673988	-3.1012738
SDSSJ000017.35+212056.0	0.0723296	21.3488827
FBQSJ0000-0851	0.072423	-8.856608
SDSSJ000017.74+020027.9	0.0739232	2.0077512
SDSSJ000020.31+040727.7	0.0846367	4.1243701
SDSSJ000021.06+012001.7	0.0877723	1.3338064
SDSSJ000021.56+171615.6	0.0898506	17.270998
SDSSJ000022.05+011742.6	0.0919044	1.295162
SDSSJ000023.59+003958.3	0.0983027	0.6661896
SDSSJ000024.70+055824.6	0.1029452	5.973513
SDSSJ000026.55+264950.8	0.110635	26.8307667
SDSSJ000030.74+045903.1	0.1281084	4.9841905
SDSSJ000035.31+310851.1	0.1471593	31.1475163

SDSSJ000036.05+041328.8	0.1502319	4.2246647
SDSSJ000036.13+282045.0	0.1505688	28.3458214
SDSSJ000036.57+243752.9	0.1524042	24.6313648
SDSSJ000037.04+032744.9	0.1543623	3.462493
SDSSJ000037.47-015515.7	0.1561412	-1.9210222
SDSSJ000037.83+112945.2	0.1576542	11.4958763
SDSSJ000039.08+272053.0	0.1628473	27.3480625
SDSSJ000040.21-020520.9	0.1675478	-2.0891378
SDSSJ000040.45+332549.9	0.1685633	33.4305153
SDSSJ000040.49+275909.4	0.1687292	27.9859722
SDSSJ000041.36+112501.2	0.1723562	11.416997
SDSSJ000046.36+000827.5	0.1931951	0.1409843
SDSSJ000046.46+143813.0	0.1936128	14.6369559
SDSSJ000046.80+024420.4	0.1950022	2.7390215
PGC1023662	0.2030556	-7.1533334
SDSSJ000048.85-062106.8	0.2035715	-6.3518863
SDSSJ000048.94+314617.0	0.2039167	31.7713947
SDSSJ000050.56-013055.2	0.2107042	-1.5153367
FBQSJ0000-1021	0.210838	-10.3655328
SDSSJ000051.33+075147.9	0.2139144	7.8632932
SDSSJ000052.63+021558.6	0.2192968	2.2662816
SDSSJ000052.87+004457.5	0.220301	0.7493188
PGC1264754	0.22564	4.186807
SDSSJ000054.46+041617.6	0.2269525	4.2715616
SDSSJ000054.95+010143.4	0.2289989	1.0287269
SDSSJ000055.53+011812.2	0.2314064	1.3033792
SDSSJ000057.79+323910.5	0.240803	32.6529274
SDSSJ000102.52+022436.2	0.260521	2.4100782
SDSSJ000102.74+012941.9	0.2614554	1.4949733
SDSSJ000103.64-011522.4	0.2651897	-1.2562148
PKS2358-161	0.2722223	-15.8519445
SDSSJ000106.93-015447.3	0.2788821	-1.9131491
SDSSJ000107.31+040436.8	0.2804611	4.0769024
SDSSJ000108.46-075239.1	0.2852859	-7.8775392
SDSSJ000109.75+053906.1	0.2906577	5.6517123
SDSSJ000113.29+300124.7	0.3054158	30.0235157
PGC1296986	0.30975	6.239466
SDSSJ000114.75+264127.6	0.3114614	26.691
SDSSJ000115.18+081503.3	0.3132624	8.2509298
SDSSJ000117.17+310715.5	0.3215503	31.120966
CRATESJ0001-0746	0.325	-7.7741667
SDSSJ000119.12+021856.1	0.3296893	2.3155699
SDSSJ000119.38+014225.9	0.3307877	1.7071826
SDSSJ000120.92+225001.0	0.3371868	22.833601
SDSSJ000122.33+204455.3	0.3430625	20.7486897
SDSSJ000122.83-050026.4	0.3451478	-5.0073209
SDSSJ000123.59-094928.9	0.3483231	-9.824688
SDSSJ000126.64+063007.0	0.3610319	6.5019512
SDSSJ000128.56-020114.6	0.3690064	-2.0207224
SDSSJ000128.89+212257.4	0.3703987	21.3826237
SDSSJ000130.19+014009.2	0.375807	1.6692274
SDSSJ000130.31+013749.2	0.3763033	1.6303405
SDSSJ000131.04+024328.0	0.3793376	2.7244413
PGC1698547	0.3847432	24.041767
TEX2358+209	0.384855	21.2267238

SDSSJ000132.64-195611.3	0.38603	-19.9364796
SDSSJ000133.80+215334.0	0.3908691	21.8927708
SDSSJ000134.02+040542.1	0.3917506	4.0950356
SDSSJ000135.36+260453.7	0.3973545	26.0815964
J000135.4-152756	0.3977778	-15.4655556
SDSSJ000139.21+204000.2	0.4133977	20.6667328
SDSSJ000139.25+024446.7	0.4135442	2.7463264
SDSSJ000142.95+310723.7	0.4289657	31.1232376
SDSSJ000143.45+041155.7	0.431063	4.1988034
SDSSJ000144.19+292305.8	0.4341393	29.3849449
SDSSJ000145.14+243234.9	0.438085	24.5430202
SDSSJ000145.14-032210.2	0.4381097	-3.3695078
SDSSJ000146.73+022425.4	0.4447089	2.4070611
SDSSJ000147.97-060412.9	0.449901	-6.0702565
SDSSJ000149.29+035708.2	0.4554018	3.9522803
SDSSJ000150.39+023830.2	0.4599938	2.6417337
SDSSJ000150.81+251129.1	0.4617094	25.1914291
SDSSJ000152.78+085141.0	0.4699188	8.861392
SDSSJ000153.58-020015.1	0.4732909	-2.0041926
SDSSJ000154.63+133955.2	0.4776482	13.6653328
SDSSJ000155.75+334829.3	0.4823199	33.8081436
SDSSJ000157.57+265204.7	0.4898849	26.8679771
SDSSJ000158.45-012256.9	0.4935442	-1.382463
SDSSJ000159.92+022738.1	0.4997005	2.4605958
SDSSJ000200.24+260148.4	0.5010317	26.0301228
SDSSJ000202.62+085628.4	0.5109434	8.9412346
PGC977300	0.5123153	-10.5105564
SDSSJ000203.63+300358.9	0.5151532	30.0663738
SDSSJ000204.51+175349.8	0.5188321	17.8971558
SDSSJ000204.95-014343.0	0.5206277	-1.7286074
SDSSJ000205.22-050118.0	0.5217558	-5.0216565
SDSSJ000205.74-080844.9	0.523945	-8.1458054
SDSSJ000206.46-014515.0	0.5269281	-1.7541575
J000207.3-374917	0.5305556	-37.8213889
SDSSJ000208.09-012632.7	0.5337103	-1.4424198
SDSSJ000208.17+232437.3	0.5340731	23.410374
SDSSJ000208.74+242014.0	0.5364302	24.3372345
SDSSJ000215.84+174801.8	0.5660139	17.8005232
SDSSJ000215.99+292352.6	0.5666413	29.3979454
SDSSJ000216.78+231704.0	0.5699292	23.2844467
SDSSJ000217.31+014729.2	0.5721623	1.7914377
SDSSJ000217.97-022437.9	0.5748819	-2.4105385
SDSSJ000218.08-022412.7	0.5753576	-2.4035151
SDSSJ000218.30+130805.8	0.5762566	13.1349344
SDSSJ000219.61+023916.0	0.5817183	2.6544414
SDSSJ000220.88+265626.4	0.587019	26.9406681
SDSSJ000220.92+021734.8	0.5872067	2.2929885
SDSSJ000221.31+015720.9	0.5888048	1.9558102
SDSSJ000223.42+124028.2	0.5976041	12.6744947
SDSSJ000225.30+010129.7	0.6054339	1.0249119
SDSSJ000225.65+021956.7	0.606895	2.3324108
SDSSJ000226.01+242955.8	0.6084152	24.4988289
SDSSJ000226.03+040145.4	0.6084878	4.0292826
SDSSJ000226.30+021744.4	0.6096086	2.2956648
MARK543	0.6102778	3.3519445

SDSSJ000227.86+222145.7	0.6160944	22.3626995
SDSSJ000228.90+013047.5	0.6204464	1.5131904
SDSSJ000229.66+041500.9	0.6235892	4.250247
SDSSJ000230.44+115555.6	0.6268703	11.9321175
SDSSJ000230.62-033140.4	0.6276115	-3.527908
BGKPN14	0.627974	0.83307
SDSSJ000233.99+295219.7	0.6416552	29.8721352
SDSSJ000234.56+032129.4	0.6440056	3.3581877
SDSSJ000236.21+104455.1	0.650887	10.7486258
SDSSJ000241.32+301249.3	0.6722034	30.2137198
SDSSJ000243.03-053025.7	0.6793312	-5.5071399
SDSSJ000245.07-012018.3	0.6878074	-1.3384148
SDSSJ000247.51-013217.5	0.6979666	-1.5381917
SDSSJ000247.60+043818.3	0.6983586	4.6384321
SDSSJ000248.01+040219.1	0.7000511	4.0386295
SDSSJ000248.60-030139.7	0.7025303	-3.0276825
SDSSJ000249.95+334213.6	0.7081253	33.7037659
SDSSJ000252.48-013236.7	0.7186828	-1.5435287
SDSSJ000252.72+125406.9	0.7196792	12.9019251
SDSSJ000253.12-075538.9	0.7213688	-7.9274802
SDSSJ000257.94+365918.4	0.7414552	36.9884453
SDSSJ000258.18+044246.3	0.742434	4.7128572
SDSSJ000300.27+015230.4	0.7511275	1.8751061
SDSSJ000301.83-062659.7	0.7576262	-6.4499176
SDSSJ000303.02-012009.7	0.7625843	-1.3360188
SDSSJ000308.10+314816.1	0.7837724	31.8044701
SDSSJ000309.49-012213.0	0.7895579	-1.3702657
SDSSJ000309.76+040353.0	0.7906737	4.0647249
SDSSJ000310.76-013028.6	0.7948348	-1.5079485
SDSSJ000311.85-012223.2	0.7994096	-1.3730993
SDSSJ000312.88+315344.4	0.8036931	31.8956566
SDSSJ000313.31+131334.8	0.8054934	13.2263493
SDSSJ000314.02+322724.1	0.8084349	32.4567169
SDSSJ000315.00+013451.7	0.812515	1.5810326
SDSSJ000315.35+331132.2	0.8139742	33.1922798
SDSSJ000316.63-201016.2	0.8193288	-20.1711578
PGC3095391	0.8202917	-27.9408611
SDSSJ000317.33+220205.8	0.8222361	22.0349369
SDSSJ000317.48+240749.0	0.8228558	24.1302776
SDSSJ000317.96+024718.1	0.8248479	2.7883606
PGC1176136	0.8258773	0.812309
SDSSJ000321.60+042552.5	0.8400243	4.4312506
SDSSJ000324.07+260054.6	0.850302	26.0151577
SDSSJ000324.64+305739.7	0.8526913	30.9610233
SDSSJ000325.40+020155.7	0.8558718	2.0321611
SDSSJ000327.21-013110.9	0.863392	-1.5196853
PGC1814347	0.8643215	27.654794
SDSSJ000327.64+200919.6	0.8652012	20.1554317
WEE3	0.8658334	-2.0044445
SDSSJ000328.32+280737.0	0.8680204	28.1269379
SDSSJ000328.82+283554.0	0.8700882	28.5983315
SDSSJ000329.74+020047.2	0.8739451	2.0131312
BGKPN3	0.8783334	1.9052778
SDSSJ000334.54-014802.3	0.8939172	-1.8006414
SDSSJ000336.30-012842.9	0.9012777	-1.4785929

SDSSJ000340.84+084332.1	0.9202068	8.7255764
SDSSJ000341.18+094744.7	0.921621	9.7957411
SDSSJ000342.15+324415.8	0.9256635	32.7377205
SDSSJ000343.56-012232.2	0.9315096	-1.3756011
SDSSJ000343.63+313645.1	0.9318168	31.6125493
SDSSJ000343.67+022129.4	0.9319775	2.3581648
SDSSJ000344.07-013631.8	0.9336558	-1.608835
SDSSJ000345.51+050708.0	0.9396422	5.1188955
SDSSJ000346.60+020640.2	0.944181	2.111173
SDSSJ000347.97-044246.6	0.9498931	-4.7129397
SDSSJ000350.08+015255.8	0.9586829	1.8821851
LBQS0001-0159	0.9633334	-1.7125
SDSSJ000351.27+024753.3	0.9636377	2.7981331
SDSSJ000353.74+321141.6	0.9739488	32.1948853
SDSSJ000354.64+371028.4	0.9776838	37.1745605
SDSSJ000355.23+001216.4	0.9801464	0.2045804
SDSSJ000355.86+014302.1	0.9827535	1.7172623
SDSSJ000355.95+020338.2	0.983155	2.060633
SDSSJ000358.31+013527.1	0.9929793	1.5908513
SDSSJ000400.37+013203.7	1.00157	1.5343496
SDSSJ000401.97+324405.2	1.0082383	32.7347641
SDSSJ000403.90+041636.0	1.0162646	4.2766767
SDSSJ000404.78-011848.7	1.0199312	-1.3135411
SDSSJ000406.06+285639.8	1.0252814	28.9443989
SDSSJ000407.75+031625.0	1.0323124	3.2736237
SDSSJ000409.09+251744.2	1.0379159	25.29562
Q0001-021	1.0381147	-1.825991
PGC1324620	1.0398434	7.5462864
SDSSJ000412.15+270133.5	1.050649	27.0259749
SDSSJ000412.15+325709.2	1.0506517	32.9525642
SDSSJ000414.21+123608.2	1.0592422	12.6022923
SDSSJ000415.20-023723.7	1.0633707	-2.6232733
SDSSJ000427.50+200126.6	1.114603	20.0240593
SDSSJ000428.16+281211.9	1.1173729	28.20331
SDSSJ000428.74+024540.3	1.1197642	2.7611852
SDSSJ000429.28+023106.9	1.1220189	2.5186026
SDSSJ000429.69+215735.9	1.1237161	21.9599819
SDSSJ000430.13+111601.1	1.1255523	11.2669802
SDSSJ000430.88+014125.0	1.1286834	1.69029
SDSSJ000431.92+034248.8	1.1330178	3.7135611
SDSSJ000433.54+372111.5	1.1397831	37.3532028
SDSSJ000439.97-000146.4	1.166559	-0.029582
SDSSJ000441.24+000711.2	1.1718389	0.1197909
SDSSJ000442.15+014141.2	1.1756563	1.6947865
SDSSJ000443.69+312612.3	1.1820818	31.4367428
SDSSJ000443.89+320627.7	1.1829003	32.1077108
SDSSJ000444.73+085805.9	1.1863955	8.9682951
SDSSJ000447.02+114719.7	1.1959192	11.7888174
SDSSJ000449.21+023552.8	1.2050748	2.5979941
SDSSJ000452.32-060611.5	1.2180064	-6.1031909
SDSSJ000453.83+001546.0	1.2243156	0.2627827
SDSSJ000453.84+104524.5	1.2243689	10.7568178
SDSSJ000455.89+033244.8	1.2329124	3.5457855
SDSSJ000456.17+000645.5	1.2340385	0.1126357
SDSSJ000456.91+000703.5	1.2371507	0.1176427

SDSSJ000457.51+070111.0	1.2396634	7.0197182
SDSSJ000458.77+023916.8	1.2448957	2.6546593
SDSSJ000501.20+102935.0	1.2550256	10.4930573
SDSSJ000501.60-012356.1	1.2567034	-1.3989187
SDSSJ000501.66+025913.9	1.2569267	2.9871869
SDSSJ000505.45-000210.8	1.272723	-0.036345
SDSSJ000506.67+081131.9	1.2778103	8.1922045
SDSSJ000507.76+212650.0	1.2823375	21.4472084
SDSSJ000509.13+323339.6	1.2880818	32.5609932
SDSSJ000509.55+023203.1	1.2898109	2.5342009
SDSSJ000511.01+234901.8	1.2958808	23.8171836
SDSSJ000512.11+001313.1	1.300496	0.220331
SDSSJ000512.18+000802.9	1.300783	0.134152
SDSSJ000512.52-000206.8	1.3021865	-0.0352338
SDSSJ000513.12+023244.4	1.3046725	2.545656
SDSSJ000514.21+120747.3	1.309222	12.1298075
SDSSJ000520.01+034740.3	1.3334104	3.7945385
2MASXJ00052124-0132306	1.3385	-1.5418333
SDSSJ000521.52-012757.7	1.3396884	-1.4660244
SDSSJ000527.51-013349.7	1.3646448	-1.5638168
SDSSJ000530.03+233428.0	1.3751414	23.5744572
SDSSJ000530.59+012235.3	1.3774998	1.3764633
SDSSJ000531.06+000950.9	1.379438	0.164165
SDSSJ000531.50+012408.9	1.3812652	1.4024662
SDSSJ000532.70+012013.1	1.3862742	1.3369689
SDSSJ000532.76+183646.4	1.3865391	18.6128883
SDSSJ000536.29+000922.7	1.4012194	0.1563286
SDSSJ000538.44-034630.7	1.4101814	-3.7751918
SDSSJ000541.29-072101.0	1.4220508	-7.3502913
SDSSJ000541.60+054424.3	1.4233401	5.7400837
SDSSJ000543.64-015320.8	1.4318516	-1.8891116
SDSSJ000544.19+171153.1	1.4341412	17.1980724
SDSSJ000545.32+063945.4	1.4388512	6.6625996
SDSSJ000547.87+023123.0	1.4494585	2.523046
SDSSJ000548.23+285512.7	1.4509584	28.9202097
SDSSJ000548.24-084808.4	1.4510083	-8.802349
SDSSJ000549.42-070824.3	1.4559189	-7.1400752
SDSSJ000549.74+300847.4	1.4572669	30.146513
SDSSJ000550.01+012338.5	1.4584069	1.3940185
SDSSJ000551.89+283729.4	1.4662207	28.6248436
SDSSJ000554.18+062138.7	1.4757829	6.3607567
SDSSJ000555.54+042345.3	1.4814509	4.3959274
S40003+38	1.4883334	38.3375
SDSSJ000558.11+193004.3	1.4921579	19.5011921
PKS0003+15	1.4968169	16.1636149
1AXGJ000605+2031	1.4975	20.5236112
SDSSJ000600.37-043639.0	1.5015777	-4.6108474
SDSSJ000600.78+093341.7	1.5032831	9.5615883
SDSSJ000603.09+061706.4	1.5129085	6.2851067
SDSSJ000605.12-042922.8	1.5213585	-4.4896536
SDSSJ000605.49+252245.3	1.5229125	25.3792381
PGC1399903	1.5351244	11.8591799
SDSSJ000608.86+211536.1	1.5369251	21.2600327
SDSSJ000609.84+365901.4	1.5410153	36.9837112
SDSSJ000610.63+021321.6	1.5443333	2.222666

SDSSJ000612.35+070150.7	1.5514945	7.0307589
J000612.6+104657	1.5525	10.7825
SDSSJ000613.29+321534.6	1.5553929	32.2596245
NRAO5	1.5578333	-6.3931389
SDSSJ000614.52+085715.4	1.5605204	8.9542856
SDSSJ000615.64+100610.1	1.5651858	10.1028042
SDSSJ000617.03+041237.2	1.5709832	4.2103233
SDSSJ000618.08+015704.2	1.5753347	1.951166
KUG0003+199	1.5813889	20.2030556
SDSSJ000619.82+020441.4	1.5826142	2.0781833
SDSSJ000621.89+323617.1	1.5912276	32.6047777
SDSSJ000622.03+255020.9	1.5918133	25.8391342
3C2.0	1.594198	-0.073455
SDSSJ000623.77-024016.6	1.5990482	-2.6712826
SDSSJ000623.97-031039.5	1.5998964	-3.1776421
SDSSJ000624.49+190338.3	1.6020514	19.0606327
SDSSJ000628.72+042826.7	1.619676	4.4740849

Table 4: Random Objects RA and Dec values in Decimal Degrees